Interactions between Fabry-Pérot and nanohole resonances in metallo-dielectric plasmonic nanostructures

Journal:	*Journal of Modern Optics*
Manuscript ID:	TMOP-2009-0134
Manuscript Type:	Regular Paper
Date Submitted by the Author:	25-Mar-2009
Complete List of Authors:	Parsons, James; University of Exeter, School of Physics Hooper, Ian; University of Exeter, School of Physics Barnes, William; University of Exeter, School of Physics Sambles, John; University of Exeter, School of Physics
Keywords:	localised surface plasmon, hole plasmon, subwavelength hole array, Fabry-Pérot, optical microcavity, fishnet structure

Interactions between Fabry-Pérot and nanohole resonances in metallo-dielectric plasmonic nanostructures

J. Parsons, I. R. Hooper, W. L. Barnes and J. R. Sambles

School of Physics, University of Exeter, Stocker Road, Exeter, EX4 4QL, United Kingdom

Abstract

We present results of numerical simulations for structures comprised of metallo-dielectric layers in which the metal layers are perforated with non-diffracting arrays of subwavelength holes, structures that are similar to the "fishnet" structures being studied as electromagnetic metamaterials. We find for visible frequencies, that such structures exhibit a stop-band in transmittance across a broad frequency range, which arises through interactions between two distinctly different types of resonant mode. Using numerical (finite element) modelling to characterise the optical response, we identify strong coupling between Fabry-Pérot resonant cavity modes within the multilayer structure and localised surface-plasmon resonances associated with the nanoholes. Our simulations show that the spectral position and width of the stop-band that occurs within the visible frequency range can be tuned by varying both the cavity spacing and the geometry of the nanohole array.

Keywords: localised surface plasmon; hole plasmon; subwavelength hole array; Fabry-Pérot; optical microcavity; fishnet structure.

1. INTRODUCTION

The etalon first proposed by C. Fabry and A. Pérot in 1899 [1], is well established as an optical transmission resonator. It consists of two parallel and partially reflecting planes separated by a fixed distance, with resonantly enhanced transmission occurring when the wavelength is approximately a half integer multiple of the cavity spacing, it has applications ranging from cavity QED [2] to the detection of gravity waves [3]. Though historically the Fabry-Pérot (FP) resonator consists of only two partially reflective separated planes, periodic multi-layer arrangements consisting of quarter-wavelength dielectric slabs of contrasting refractive indices also demonstrate similar resonant transmission features [4]. The optical response of such a structure exhibits two distinct regimes, high reflectivity in the stop-bands or high transmissivity in the pass-bands. The spectral shape of the reflectance / transmittance is governed by the number of periods within the structure, and pass-bands across a narrower frequency range can be achieved by placing two or more of these cavities together to form a series of coupled resonators [5]. With advances in fabrication technology, the possibility of investigating more elaborate multilayer structures arose, such as those incorporating metallic layers or containing a high number of periods. In 1939, W. Geffcken [6] fabricated metallo-dielectric thin-film stacks, which offered a number of advantages over all-dielectric stacks. The observed transmission resonances from a metallo-dielectric structure were significantly narrower in spectral width than those previously studied in all-dielectric structures, a result of the high reflectivity of the metal layers. Recently, in a structure consisting of multiple Ag / MgF_2 periods [7,8], it was shown that the pass-band regions are highly tunable. It was also demonstrated that the resonant transmission is several orders of magnitude greater than a single metal film of the equivalent thickness. Metallo-dielectric structures have been studied extensively in recent years for a number of uses, including non-linear optical applications [9-12] and negative refraction [13,14]. Variant structures in which the metallic layers are not continuous but rather have a "fishnet" structure, not so dissimilar to the structures examined here, are also being keenly pursued as electromagnetic metamaterials [15-18].

Whilst FP-type resonances are one example of an electromagnetic mode that is supported by a periodic nano-structure, many others exist. For example, if we consider metallic films perforated with arrays of holes, different types of resonant modes may also be supported. For an optically thick metal film perforated with an array of subwavelength holes, significantly enhanced transmission has been observed [19-20]. In these structures, the period of the array is of order the wavelength of light. This is an essential requirement, since the array is used as a mechanism to scatter the incident light, allowing the excitation of surface plasmon-polaritons (SPPs) on the surface of the metal layer. More recently a second mode associated with hole arrays has been explored. The localised surface plasmon resonance (LSPRs) that is widely studied in metallic nanoparticles has also been identified in nanohole structures [21-24]. For arrays of nanoholes with a periodicity short enough that they are non-diffracting (i.e. zeroth order for frequencies in the vicinity of the LSPRs), the electromagnetic coupling between holes leads to a significant modification of the optical response when compared to an isolated hole [25].

In this letter, we consider multilayer structures which have been perforated with *non-diffracting* arrays of holes supporting LSPRs exhibiting a series of FP-type transmission resonances. This leads to some unusual properties in the optical response; notably a stop-band in transmission occurring across a wide range of visible frequencies. The stop-band is centred at the LSPR frequency observed for a single layer of holes, and is accompanied by significant absorption. It is shown that the spectral width and centre frequency of the stop-band can be tuned by adjusting the cavity spacing and array periodicity, making these structures useful in optical filter applications. We also identify a shift in frequency of the FP modes as a result of strong interactions between LSPR and FP modes, which is verified by the simulated dispersion of the modes.

2. RESULTS AND DISCUSSION

We first consider the optical response of a planar Ag film with thickness 20 nm (figure 1), and subsequently perforate this with an infinite square array of cylindrical holes having diameter 60 nm and period 150 nm (as shown in the inset of figure 1). The structure is simulated using commercial finite

element software (HFSS from Ansoft Corporation) with a mesh size of 4.5 nm, and is illuminated at normal incidence. The surrounding medium is glass (refractive index n_r = 1.52, n_i = 0.00) and is assumed to be non dispersive over the frequency range of interest, whilst the permittivity values for silver were taken from reference data [26]. The perforated structure in figure 1 shows a distinct transmittance minimum for incident light of frequency 545 THz (λ_{vac} = 550 nm). At a similar frequency, the absorbance spectrum also shows a clear maximum which is linked to the transmittance minimum. We attribute these transmittance minima / absorbance maxima to the coupling of incident light to dipolar LSPR modes associated with holes in the array, in a manner analogous to that of LSPRs in metallic nanoparticles [21-25].

In figure 2, we use a scattering matrix approach [27] to simulate the optical response of a periodic structure consisting of five planar Ag layers (thickness 20 nm) separated by 110 nm of glass, illuminated at normal incidence with glass surrounding medium (refractive index n_r = 1.52 n_i = 0.00). The transmittance and absorbance spectra shows the four first-order resonant FP modes of the structure, and a partial transmission (pass-band) region for frequencies in the range 475 THz – 750 THz (λ_{vac} = 630 nm – 400 nm). As discussed elsewhere [28], the width of the pass-band region is known to be independent of the number of layers, and is determined only by the metal and cavity thicknesses forming the unit cell. The pass-band region originates from a resonant tunnelling mechanism associated with evanescent fields in the Ag layers coupling to cavity resonances in the glass layers. Within the Ag layers, the evanescent fields can undergo successive reflections at the Ag-glass interfaces, giving rise to standing field solutions with either a *cosh* or a *sinh* distribution function. At the boundary these must couple to *cos* or *sin* oscillations within the cavity. In the inset of figure 2, we plot the time-averaged electric field magnitude as a function of position for a cross section taken perpendicular to the metal-glass interfaces. The upper inset shows the distribution at the high frequency band edge, whilst the lower inset is for the low frequency band edge. At the high frequency band edge (the FP mode at 660 THz (λ_{vac} = 454 nm)), fields in adjacent cavities oscillate out of phase and the majority of field enhancement occurs within the cavity region. Only a relatively small amount of the oscillation occurs within the metal layer, with the

nodes corresponding to the lowest order resonant mode occurring slightly inside the metal, not at the interface as would be expected for a perfect conductor. Equations 1a and 1b can be used to determine the resonant wavelength / frequency for the ideal case of quantised standing wave modes between two perfectly reflecting surfaces. In these equations, n is the refractive index of the medium within the cavity, L is the cavity length in metres, c is the speed of light in vacuum and N is the Nth order resonant mode.

$$\lambda_N = \frac{2nL}{N} \qquad \textbf{(1a)}$$

$$f_N = \frac{cN}{2nL} \qquad \textbf{(1b)}$$

It should be noted that in the ideal limit of perfectly conducting films the electromagnetic fields are completely reflected and cannot penetrate the cavity in the first instance, rendering coupling to the cavity mode impossible. However using equations 1a and 1b to consider this hypothetical, ideal scenario, we predict a lowest order resonant frequency of 900 THz (λ_{vac} = 333 nm). In the structure shown in figure 2, the Ag layers have a finite conductivity and the FP mode at the high frequency band edge occurs at 660 THz (λ_{vac} = 454 nm). At the low frequency band edge (in figure 2 the FP mode at 440 THz (λ_{vac} = 680 nm)), the discrepancy with the ideal case is larger, since fields in adjacent cavities oscillate in phase and a significant proportion of the oscillating field is within the Ag layers. The effective wavelength of this oscillation extends significantly beyond the Ag-glass interfaces, and so the effective cavity length is significantly larger than the physical cavity length L in Equations 1a and 1b.

We now consider a structure which incorporates features from both figure 1 (non-diffracting arrays of holes) and figure 2 (a multilayer metallo-dielectric planar stack). In figure 3, the simulated transmittance and absorbance spectrum is plotted for a planar structure consisting of 5 layers of Ag with

thickness 20 nm separated by 110 nm, perforated with an infinite array of cylindrical holes with 60 nm diameter and 150 nm periodicity. In figure 4, the magnitude of the simulated absorbance has been plotted as a function of frequency and incident angle ($\sin\theta$) in order to map the simulated dispersion of the modes supported by the structure. This is shown for the case of illumination with transverse electric (TE) polarised light (Our simulations have also explored the dispersion of the modes when illuminated with transverse magnetic (TM) polarised light, the results of which are very similar to those of the TE polarised light and as such only the TE results are presented here).

There are a number of spectral features which immediately suggest interactions between LSPR and FP modes. As with the planar structure, a series of transmittance maxima are observed in figure 3; however, at normal incidence these are separated by a stop-band centred around 540 THz (λ_{vac} = 555 nm). It is possible to identify similarities between the nature of the stop band and the optical characteristics of the LSPR for the single layer of holes in figure 1. The centre frequency of the stop band in figure 3 is in close agreement with the LSPR frequency observed for a single layer of holes. The width of the stop band is also similar to that of the transmittance minima / absorbance maxima which are attributed to the coupling of incident light to LSPRs in the single layer of holes. In comparison with the planar multilayer structure, a shift in frequency of the FP modes is observed, which is dependent on the relative frequencies of both the individual FP modes and the LSPR of the hole. The dispersion of the mode associated with the LSPR in figure 4 shows a relatively flat-band at a frequency of 510 THz (λ_{vac} = 588 nm) with absorption close to unity.

A note should be made here regarding the spectral form of the resonances in absorption and transmission, as seen in figures 1-4, as this will be important when discussing the stop-band in transmission. Unsurprisingly, both the FP resonances and the LSPR hole resonance are identified by resonant absorption features (figure 4). However, the fields associated with the FP modes are localised within the cavity, resulting in a higher than off-resonance field strength on the transmission side of the structure (see figures 2(a) and (b)). Thus resonant transmission peaks (just as from standard FP etalons)

are observed upon their excitation. Conversely, the resonance associated with the holes is a highly localised mode confined to the metal film, resulting in an increase in absorption and a decrease in transmission. Simplistically, the form of the transmission curves in figure 3 can now be readily understood as resulting from FP-type transmission maxima distributed across the frequency range, with a transmission minimum at 550 THz (λ_{vac} = 545 nm) arising from the LSPR hole resonance. However, a more complete understanding can be gleaned from investigating the dispersion of the modes in figure 4.

Whilst the three higher frequency modes above the horizontal LSPR disperse as a function of angle in a manner consistent with their being FP type modes, there is a clear interaction between the modes occurring at a lower frequency than the LSPR, and the LSPR. Closer inspection of figure 4 shows that the resonance associated with the hole is situated amongst what appears to be five FP modes. Given that the structure consists of only four cavities, and as such one would expect only **four** first-order FP modes to be observed, our observation of what would appear to be five modes is unexpected. In order to explain the origin of this apparent additional mode, we have performed modelling of both perforated and planar 20 nm thick Ag layers separated by a dielectric layer (a simpler, 3 layer system, as opposed to the 7 layer system studied for figure 4), calculating their absorbance as a function of frequency and dielectric layer thickness for normally incident light (figure 5). On inspection of these two plots the origin of the additional mode now becomes apparent: The first order FP mode, which for the planar system disperses from 300 THz (λ_{vac} = 1000 nm) for a layer spacing of 250 nm to approximately 700 THz (λ_{vac} = 428 nm) for a layer spacing of 50 nm, interacts strongly with the LSPR such that for some range of layer spacings (including 110 nm, as studied in figure 4) there appears to be three modes, with two of them corresponding to the first order FP mode which straddles the LSPR. With this knowledge we can identify all of the modes evident in figure 4; an LSPR and 4 FP modes, one of which is straddling the LSPR mode resulting in it appearing to be two distinct modes.

As mentioned previously, and as clearly evident in figure 4, the two lower frequency FP modes tend towards the LSPR frequency with increasing angle of incidence, whilst FP modes above this frequency continue to follow the expected FP-type dispersion. A consequence of this is that the frequency gap between the FP-type modes above the LSPR and those below it widens as the angle of incidence is increased, with a corresponding increase in the width of the transmission stopband. For example, at sin θ = 0.8 in Figure 4, the width of the stop-band has more than doubled relative to that which is observed at normal incidence, such that it occurs across the frequency range ~500 THz – 660 THz (λ_{vac} = 600 nm – 454 nm).

It has been previously shown that the resonant frequencies of LSPR and FP modes can be tuned [8-9,25,28]. Since we have identified that the transmittance stop-band originates through the interaction between these modes, it should be possible, in principle, to modify the respective resonances such that the stop-band can occur across any desired frequency range. To demonstrate this tunability, we consider a structure consisting of 5 periods of 20 nm Ag / 140 nm glass, perforated with an array of 90 nm diameter holes with periodicity 225 nm. The simulated transmittance spectrum is shown in figure 6, where the stop-band has been shifted in frequency relative to the previous structure of 60 nm diameter holes, and is observed across frequencies in the range 440 THz – 495 THz (λ_{vac} = 681 nm – 606 nm). In this instance, a variation in the array geometry modifies the coupling strength between hole LSPRs, leading to a red-shift in the resonant frequency of the LSPR. Similarly, increasing the thickness of the dielectric cavity region leads to a red-shift of frequencies within the pass-band.

3. CONCLUSIONS

We have identified a distinct stop-band in the transmittance of metallo-dielectric one-dimensional photonic band gap structures which have been perforated with non-diffracting arrays of holes. By considering both a single Ag layer perforated with holes, and a planar Ag-glass multilayer stack, we have shown that the stop-band originates through coupling between FP resonances and LSPRs

associated with the holes. We have also demonstrated that the central frequency and width of the stop-band can be suitably tuned by modifying the resonant frequencies of the FP modes and the hole LSPRs. This high degree of tunability of the stop-band at visible frequencies in such structures is a desirable property for optical filter applications, it might perhaps also find relevance in designing fishnet-type electromagnetic metamaterials.

ACKNOWLEDGEMENTS:

This work was supported through funding from Hewlett Packard (Bristol) in association with Great Western Research (http://www.gwr.ac.uk). WLB has the pleasure of acknowledging the Royal Society for support through a Merit Award.

References:

1 C. Fabry and A. Pérot, *Annales de Chimie et de Physique* **1899**, 115-144.
2 A. L. Schawlow and C. H. Townes, *Physical Review* **1958**, *112*, 1940-1949.
3 G. Brodin and M. Marklund, *Classical and Quantum Gravity* **2003**, *20*, 41-51.
4 A. H. Pfund, *Journal of the Optical Society of America* **1934**, *24*, 99-102.
5 H. A. Macleod, *Thin Film Optical Filters;* Hilger: London, 1969.
6 W. Geffcken, *Deutsches Reich Patentschrift* **1939**, 716153.
7 M. C. Larciprete, C. Sibilia, S. Paolini and M. Bertolotti, *Journal of Applied Physics* **2003**, 93, 5013-5017.
8 M. Scalora, M. J. Bloemer, A. S. Pethel, J. P. Dowling, C. M. Bowden and A. S. Manka, Journal of Applied Physics **1998**, 83, 2377-2383.
9 J. M. Bendickson, J. P. Dowling and M. Scalora, *Physical Review E* **1996**, 53, 4107-4121.
10 M. Scalora, J. P. Dowling, C. M. Bowden and M. J. Bloemer, *Journal of Applied Physics* **1994,** 76, 2023-2026.
11 C. M. de Sterke and J. E. Sipe, *Physical Review A* **1988**, 38, 5149-5165.
12 D. N. Christodoulides and R. I. Joseph, *Physical Review Letters* **1989**, 62, 1746-1749 (1989).
13 M. Scalora, G. D'Aguanno, N. Mattiucci, M. J. Bloemer, D. de Ceglia, M. Centini, A. Mandatori, C. Sibilia, N. Akozbek, M. G. Cappeddu, M. Fowler, and J. W. Haus., *Optics Express* **2007,** 15, 508-523.
14 J. Gerardin and A. Lakhtakia, *Microwave and Optical Technology Letters* **2002**, 34(6), 409-411.
15 G. Dolling, M. Wegener and S. Linden, *Optics Letters* **2007**, 32, 551-553.
16 N. Liu, L. Fu, S. Kaiser, H. Schweizer and H. Giessen, *Advanced Materials* **2008**, 20, 3859-3865.
17 J. Valentine, S. Zhang, T. Zentgraf, E. Ulin-Avila, D. A. Genov, G. Bartal and X. Zhang, *Nature* **2008**, 455, 376-379 (2008).
18 C. M. Soukoulis, J. F. Zhou, T. Koschny, M. Kafesaki and E. N. Economou, *Journal of Physics: Condensed Matter* **2008**, 20, 304217.
19 T. W. Ebbesen, H. J. Lezec, H. F. Ghaemi, T. Thio and P. A. Wolff, *Nature* **1998**, 391, 667-669.
20 W. L. Barnes, W. A. Murray, J. Dintinger, E. Devaux and T. W. Ebbesen, *Physical Review Letters* **2004**, 92, 107401.
21 J. Prikulis, P. Hanarp, L. Olofsson, D. Sutherland and M. Kall, *Nano Letters* **2004**, 4, 1003-1007.
22 T. Park, N. Mirin, J. Lassiter, C. Nehl, N. Halas and P. Nordlander, *ACS Nano* **2008**, 2, 25-32.
23 T. Rindzevicius, Y. Alaverdyan, B. Supuvelda, T. Pakizeh, M. Kall, R. Hillenbrand, J. Aizpurua and F. J. Garcia de Abajo, *Journal of Physical Chemistry* **2007**, 111, 1207-1212.
24 S. H. Chang, S. K. Gray and G. C. Schatz, *Optics Express* **2005**, 13, 3150-3165.
25 J. Parsons, E. Hendry, C. P. Burrows, B. Auguié, W. L. Barnes and J. R. Sambles, *Physical Review B* **2009**, 79, 073412.
26 E. D. Palik, *Handbook of optical constants of solids;* Academic: New York, 1985.
27 D. Ko and J. R. Sambles, *Journal of the Optical Society of America A* **1988**, 5, 1863-1866.
28 M. R. Gadsdon, J. Parsons and J.R. Sambles, *Journal of the Optical Society of America B* **2009**, 26(4), 734-742.

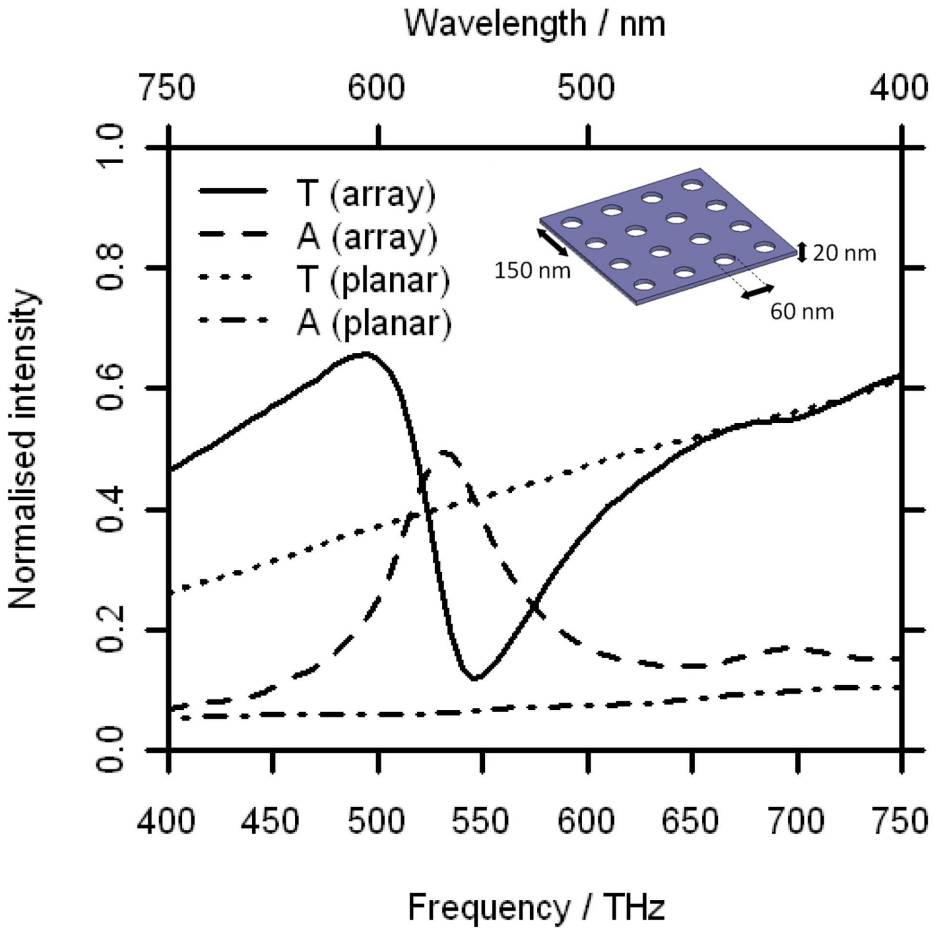

Figure 1. Simulated transmittance and absorbance spectra at normal incidence for a planar Ag layer (20 nm thickness) and a Ag layer (20 nm thickness) perforated with an infinite square array of 60 nm diameter cylindrical holes with periodicity 150 nm (shown in the inset). The surrounding medium has refractive index $n_r = 1.52$, $n_i = 0.00$.
87x87mm (600 x 600 DPI)

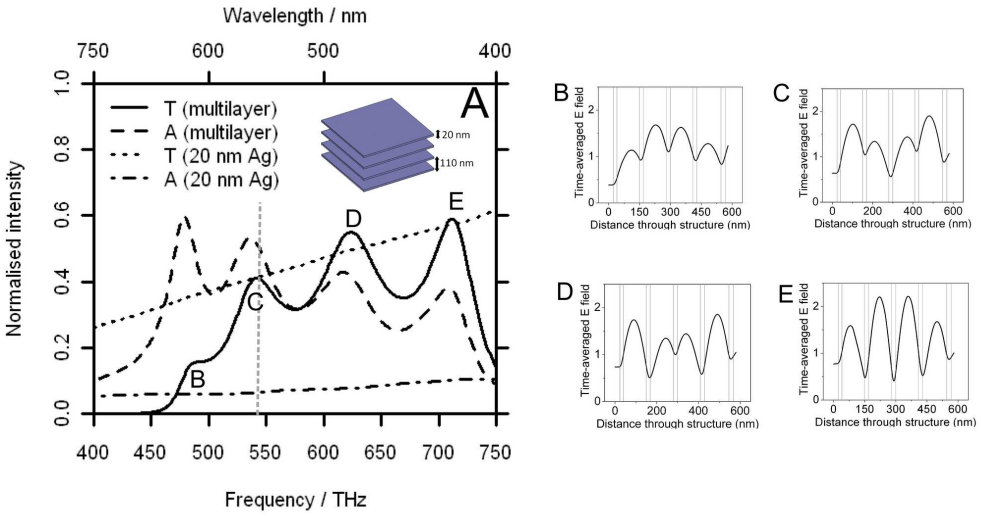

Figure 2. Simulated transmittance and absorbance spectrum at normal incidence for a planar Ag layer (20 nm thickness) and a multi-layer structure consisting of 5 layers of 20 nm Ag separated by 110 nm (A). The surrounding medium has refractive index $n_r = 1.52$, $n_i = 0.00$. The grey line illustrates the resonant frequency for a single layer of 20 nm Ag perforated with holes having diameter 60 nm and periodicity 150 nm. The inset figures (B-E) show the time-averaged electric field magnitude at the resonant frequencies of the FP modes for a cross section taken perpendicular to the stack.
85x46mm (600 x 600 DPI)

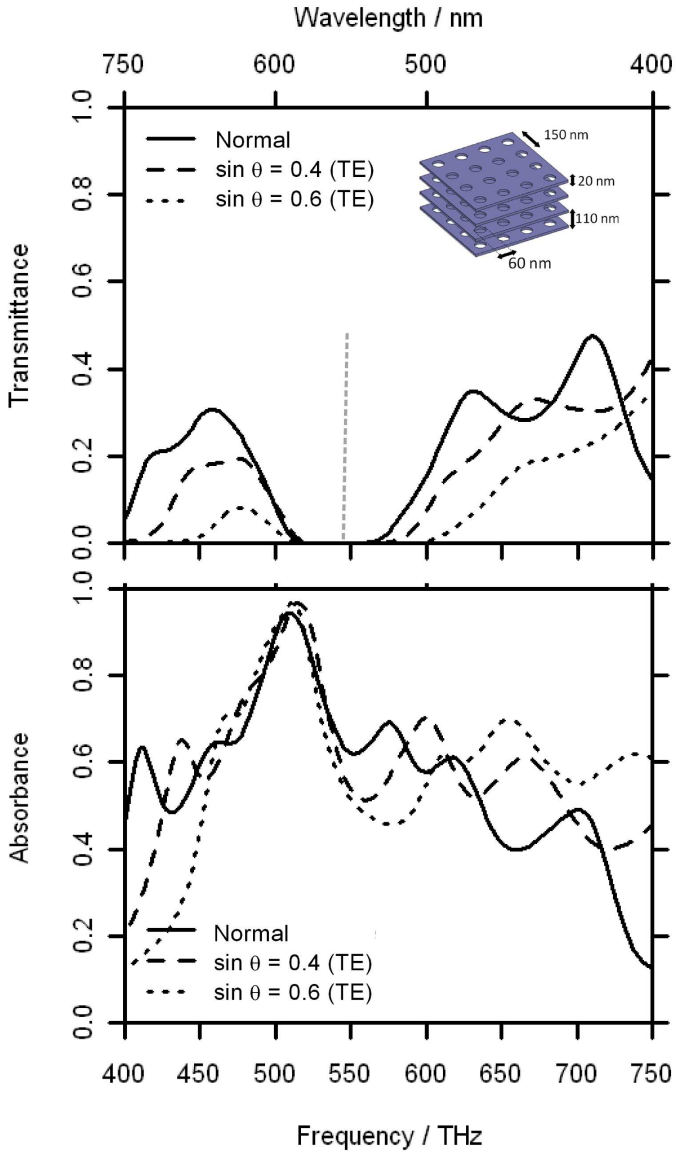

Figure 3. Simulated transmittance and absorbance spectra for a planar structure consisting of 5 layers of Ag with thickness 20 nm separated by 110 nm, perforated with an infinite square array of cylindrical holes with 60 nm diameter and 150 nm periodicity. The surrounding medium has refractive index $n_r = 1.52$, $n_i = 0.00$. The solid line corresponds to illumination at normal incidence, the dashed and dotted lines correspond to illumination with TE polarised light at angles 23.5° ($\sin\theta = 0.4$) and 36.9° ($\sin\theta = 0.6$) respectively. The grey line at 545 THz represents the resonant frequency for a single layer of Ag perforated with an identical array of holes (see figure 1).
137x228mm (600 x 600 DPI)

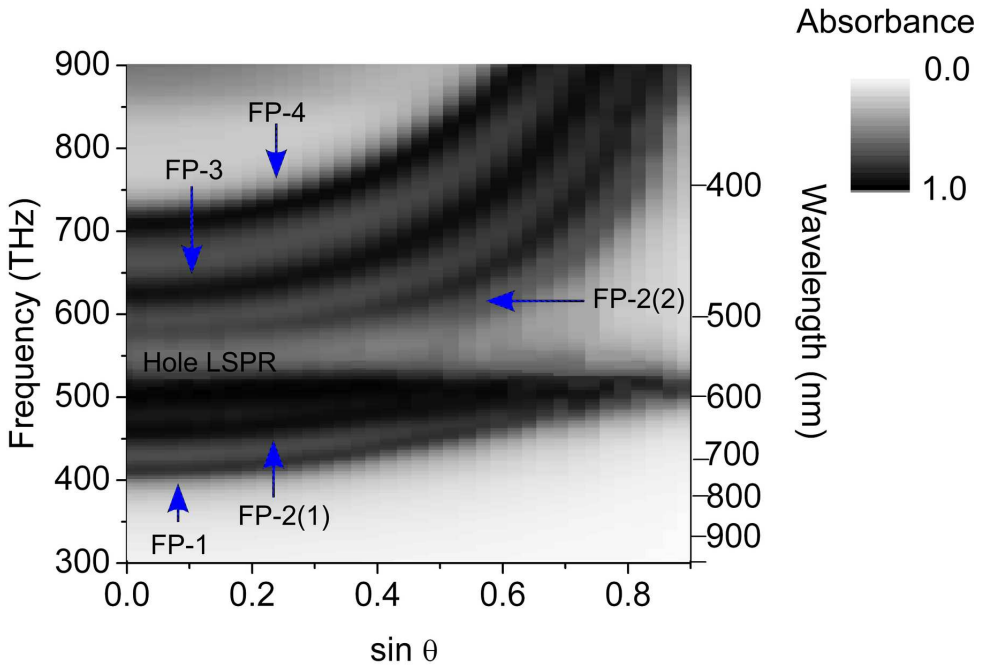

Figure 4. Contour plot showing the magnitude of the simulated absorbance as a function of frequency and sin θ (where θ is the incident angle) for TE polarised light illuminating a structure consisting of 5 layers of Ag with thickness 20 nm separated by 110 nm, perforated with an infinite square array of cylindrical holes with 60 nm diameter and 150 nm periodicity. The surrounding medium has refractive index n_r = 1.52, n_i = 0.00.
79x54mm (600 x 600 DPI)

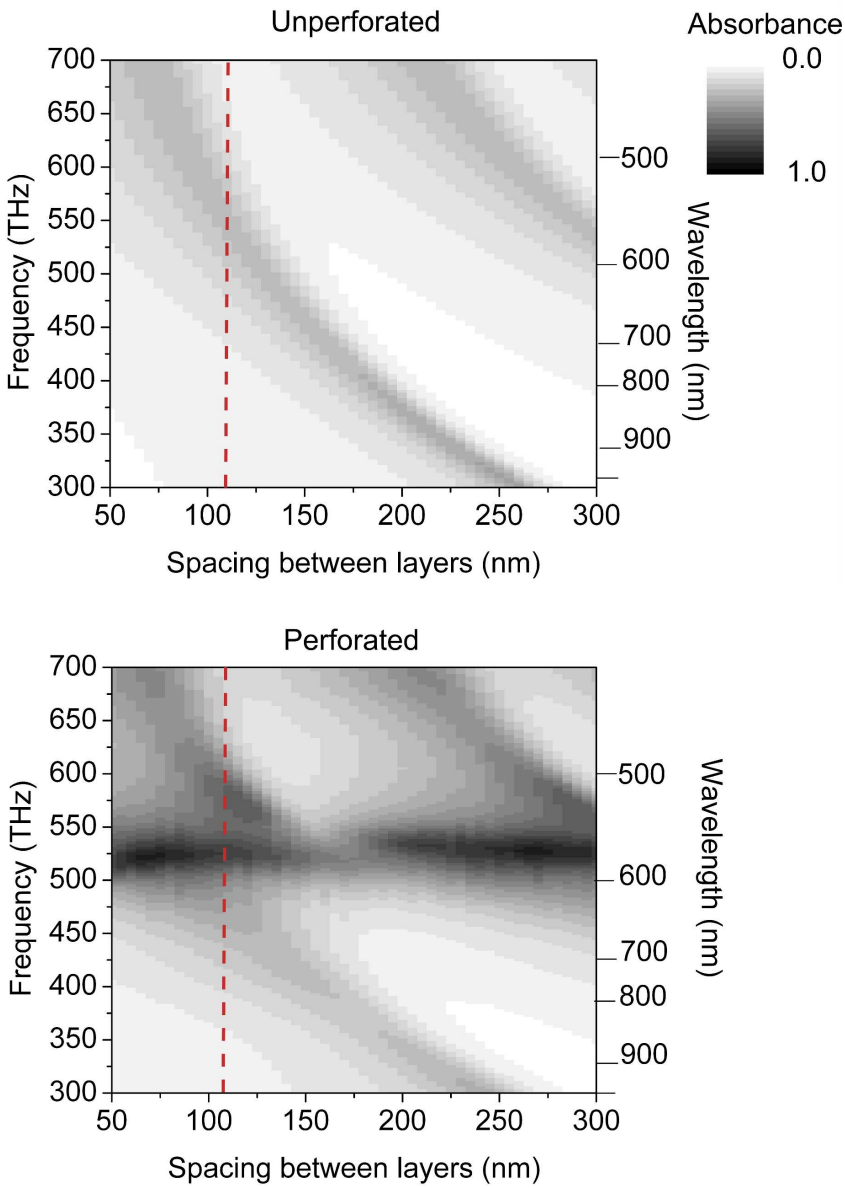

Figure 5. The magnitude of the simulated absorbance is plotted as function of frequency and spacing between two unperforated (top) and perforated (bottom) Ag layers with thickness 20 nm. The perforated structure consists of an infinite square array of cylindrical holes with diameter 60 nm and periodicity 150 nm. The results are for normal incidence, with the surrounding medium having refractive index $n_r = 1.52$, $n_i = 0.00$. The dashed line represents the separation of the metal layers in the structures described in Figures 2 and 3.
157x222mm (600 x 600 DPI)

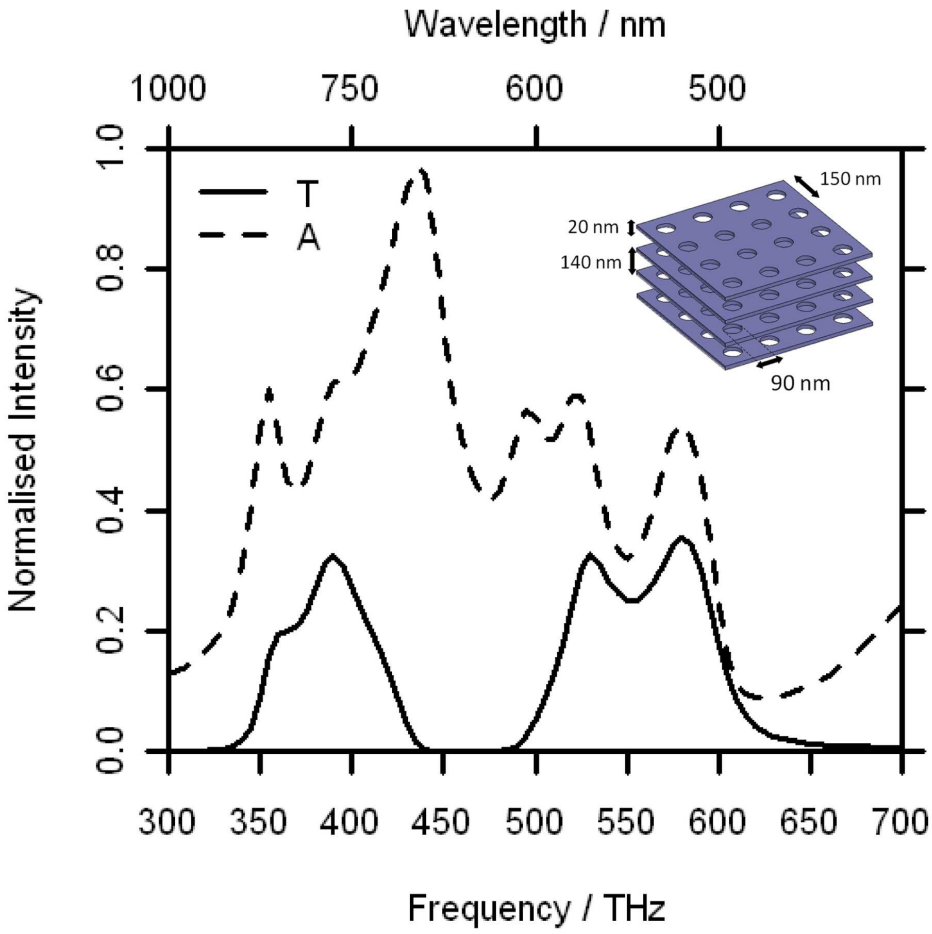

Figure 6. Simulated transmittance and absorbance spectrum at normal incidence for a planar structure consisting of 5 layers of Ag with thickness 20 nm separated by 140 nm, perforated with an infinite square array of cylindrical holes with 90 nm diameter and 150 nm periodicity. The surrounding medium has refractive indices $n_r = 1.52$, $n_i = 0.00$.
82x82mm (600 x 600 DPI)